Analytical Methods

Accepted Manuscript

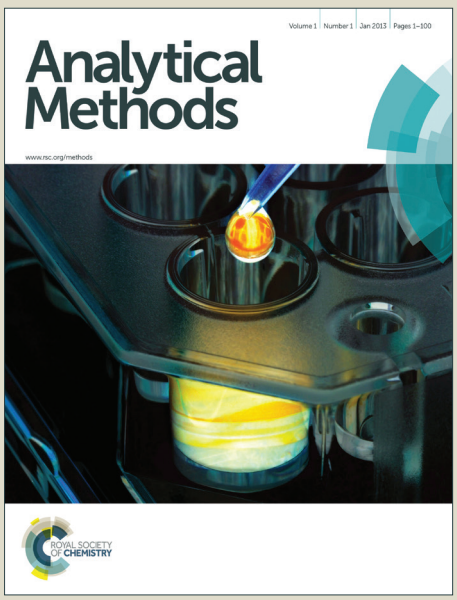

ROYAL SOCIETY OF CHEMISTRY

www.rsc.org/methods

Journal Name

RSCPublishing

ARTICLE

Second-order advantage achieved with the aid of gold nanoparticle catalytic activity. Determination of nitrophenol isomers in binary mixtures

Faride Rabbani,[a] Hamid Abdollahi[a]* and M. Reza Hormozi-Nezhad[b]*,

Cite this: DOI: 10.1039/x0xx00000x

DOI: 10.1039/x0xx00000x

www.rsc.org/

A novel, simple and rapid spectrophotometric method for the determination of nitrophenol (NP) isomers mixtures, based on catalytic activity of gold nanoparticles was described. Gold nanoparticles (~13 nm) solution was used to catalyze the reduction of NP isomers to aminophenols by an excess amount of $NaBH_4$. The second-order data was obtained by spectrophotometric monitoring the reduction process of NP isomers. So, multivariate curve resolution optimized by alternative least squares (MCR-ALS) was used to analyze such data. MCR-ALS, an appropriate second-order method, can exploit the so called 'second order advantage' (the ability to determine in the presence of uncalibrated interferences). With the use of this multivariate curve resolution method, we applied a single calibration sample, instead of a large number of calibration samples. The results obtained by MCR-ALS analysis were in good agreement with true concentration of NP isomers. Furthermore, the ranges of all possible concentrations of NP isomers were obtained calculating all feasible solutions. These ranges of concentrations are the all amounts which, each of them, may be achieved applying different initial estimates in MCR-ALS. The proposed procedure was further applied to determine the NP isomers spiked in dam water samples, and it showed good promise for quantitative detection of NP isomers.

Introduction

Metal nanoparticles have received much attention during the past several decades as they play important roles in various areas of materials science. These metal nanoparticles, especially gold nanoparticles, have been widely exploited in catalysis[1, 2], biosensing[3], and optics[4] due to their interesting physicochemical and optoelectronic properties.

Catalysis is one of the most important chemical applications of metal nanoparticles. Among the metallic nanoparticles, gold nanoparticles have drawn great scientific interest because of their application as heterogeneous catalyst in various liquid-phase catalytic processes. However, gold was less well studied in the catalysis field because it was considered chemically inert and, therefore, uninteresting for many years. However, ever since Hutchings' discovery that gold is the catalyst of choice for acetylene hydrochlorination[5] and Haruta's discovery that gold nanoparticles supported on a certain kind of support are very active for CO oxidation at low temperatures.[6] the study of the catalytic properties of gold nanoparticles has been booming.[7] Gold, and other noble metal e.g. Pt, Ir, become highly reactive when they attain nanosized domain, because in the nanometer size range, the bulk properties of a metal change.[8] Therefore, one major reason for neglecting or ignoring gold catalysis for many years is that in most cases, supported gold particles prepared by the traditional incipient-wetness impregnation method exceed a critical nanosize range outside of which the gold catalysts are not active. One of the gold nanoparticle applications in the catalytic field is the catalytic reduction of nitro components. The reduction of nitro compounds to amino compounds with an excess amount of $NaBH_4$ has often been used as a model reaction to examine the catalytic performance of metal nanoparticles, as well as the

gold nanoparticles, due to the simple procedure and easily available equipment.[9]

Nitrophenol is a family of Aromatic compounds containing nitro groups with three isomers, *o*-nitrophenol (*o*-NP), *m*-nitrophenol (*m*-NP) and p-nitrophenol (*p*-NP). They are important chemicals, having wide usage in the manufacture of pesticides, explosives and dyestuffs, plasticizers and pharmaceuticals etc.[10] Nitrophenols are found widely as environmental pollutants in soil, freshwater, marine environments and in the atmosphere, which coming from pesticide and fungicides degradation products, car exhausts, industrial wastes, and degradation of lignin and humic acids present in soils. Because of their toxic effects on humans, animals and plants, they are categorized as the hazardous waste and priority toxic pollutant by U.S. EPA.[11] However, the toxicities of nitrophenol isomers are different with each other. As, *o*-NP and *p*-NP are highly toxic and exhibit much more serious effects on the growth and metabolic activities of the organism.[12] Due to the vast scale distribution in the environment, determination of nitrophenol isomers has become one of the important goals of environmental analysis. These compounds have few structural differences and similar chemical properties therefore; they will interfere with each other during determination. So, differentiating structural and simultaneous determination is a challenging and critical work in analytical chemistry, pharmaceutical industry and environmental monitoring. Till now, so many methods such as chromatography[13], electrochemistry[14] and spectroscopy methods[15] have been employed for recognition or detection of NPs, but few reports concern simultaneous determination of these isomers.[15-18]

In this study, reduction of NP isomers by gold nanoparticles as catalysts, gave us an opportunity to achieve second-order data. In comparing to previous mentioned works, as the first time, we successfully applied second-order multivariate curve resolution to the quantitative analysis of mixtures of nitrophenol isomers. Quantitative determination of analyte in the presence of uncalibrated interference was appropriately achieved.

Prediction of the analyte concentration in the presence of the unknown interferent, is an inherent valuable property of second-order data, which, is known as the second-order advantage.[19] The proposed procedure for determination of nitrophenol isomers, has many advantages over first-order multivariate calibration procedures. A single standard, that containing the analyte of interest, is enough to achieve quantitation when spectroscopic and reduction kinetic behavior are both simultaneously taken into account. Second-order data is produced by instruments that give two dimensional responses or matrix for each sample, instead of one dimensional responses. Here, second-order data is obtained by recording the kinetic UV-Vis spectra related to the catalytic reduction of nitrophenols. There are some report on using kinetic second-order data in order to simultaneous determination of mixtures, such as pesticides and metal ions[20, 21].

Many appropriate second-order methods, used to resolve multicomponent mixtures such as MCR-ALS[22], PARAFAC[23], GRAM[24] and etc, have the ability to provide second-order advantage. The applications of soft-modeling methods in second-order calibration have been demonstrated in different publications[25-29] and it is proved to be a powerful technique for quantification of complex mixtures. However, the main limitation of all MCR methods is the rotational ambiguity which is known and documented since the very beginning of chemometrics.[30] For quantitative analysis, we employed the systematic grid search algorithm in two component systems as a soft-modeling method. In this approach all feasible solutions (a range of concentrations) were obtained for unknown sample, which it was augmented with a standard sample of analyte of interest. In addition to achieve second-order advantage, the proposed approach is very simple and rapid, where, the kinetic process of reduction was completed in 8 minutes. This method was successfully applied to analyze the synthetic and spiked dam water samples in different binary mixtures of nitrophenol isomers.

Experimental

Materials and reagents

Hydrogen tetrachloroaurate ($HAuCl_4$, 99%) and Sodium citrate (99%) were purchased from Sigma–Aldrich. Sodium Chloride (NaCl) and Sodium borohydride ($NaBH_4$) were purchased from Merck. Nitroaromatics, viz. *p*-nitrophenol (*p*-NP), *m*-nitrophenol (*m*-NP) and *o*-nitrophenol (*o*-NP), were obtained from Sigma–Aldrich. Water was purified with a Milli-Q water system.

Instrumentation and software

The absorption spectrum of each solution was recorded with a Scinco S-2100 Photodiode Array UV-vis spectrophotometer with a fixed slit width of 2 nm. Each original kinetic data was arranged into a matrix format Y (I×J), where I is the number of rows (number of measured spectra over times) and the J is the number of columns (number of measured wavelengths). The data were analyzed using MATLAB software, version 6.5. The TEM images of citrate-capped gold nanoparticles were obtained by using a Hitachi H-9000NAR transmission electron microscope, operating at 200 kV.

Synthesis of colloidal gold nanoparticles

The citrate-capped gold nanoparticles was prepared following the well-documented Frens' method.[31] The desired size of gold nanoparticles in this reductive synthesis were determined adjusting the amount of citrate to $HAuCl_4$ ratio. A standard procedure for preparing gold nanoparticles of 13 nm diameter (Au_{13nm}) is as follows. Briefly, a 50 ml aqueous solution of $HAuCl_4$ (0.5 mM) was heated to boiling with vigorous stirring and 5 ml of trisodium citrate (1%) was added all at once. The yellow solution turned clear, dark blue and then a red color

within a few minutes. The solution was heated for an additional 30 min after the red color was observed. The solution was then removed from heat and kept stirring for 15 min. After that the solution was set aside to cool down to room temperature. The particle size determined by transmission electron microscopy (TEM) was 13.6 nm, (see Fig. 1). Concentration of as-prepared Au_{13nm} is 3.7 nM.

Sample collection and preparation

The UV-Vis spectra were collected over the range of 250-600 nm during kinetic process of the reductions. Briefly, certain amount of *p*-, *m*- or *o*-nitrophenol stock solution (as standard sample) or binary mixture of them (as unknown sample) was mixed with deoinized (DI) water up to 2.9 mL in a standard cuvette having 1-cm path length as a batch chemical reactor. Afterward, 100 µL of 0.5 M freshly prepared solution of $NaBH_4$ as hydrogen source was added and the mixture was mixed well and allowed to react for 3 min. Finally, 30 µL of as prepared solution of gold nanoparticles was introduced to start the reduction, and time-dependent absorption spectra were recorded immediately after the addition of gold nanoparticles. The first spectrum, after the addition of gold nanoparticles was recorded at 10 s and after that the spectra were recorded every 5 s to 3 min, and then every 10 s to 8 min. All reactions were carried out at 25 °C.

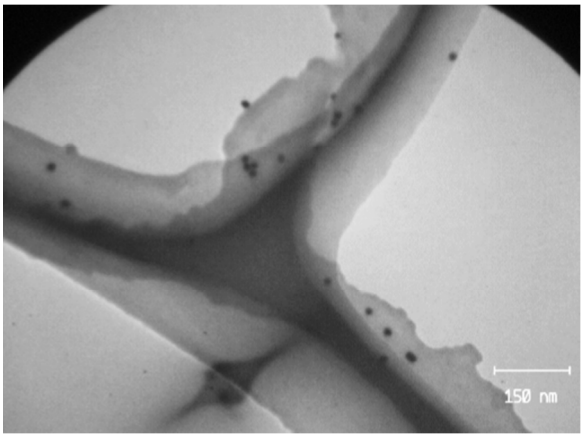

Fig. 1 TEM images of the citrate-capped gold nanoparticles, with the average diameter of 13.6 nm.

Results and discussion

Gold nanoparticles catalytic activity

Catalytic activity of gold NPs, as one of the main applications, has been interested considerably in recent years. Herein, the reduction of nitrophenol isomers (*o*-NP, *m*-NP and *p*-NP) to corresponding aminophenol is achieved using 13 nm gold nanoparticles and $NaBH_4$ as the reducing agent. Fig. 2A-C show the absorption spectra of individual nitrophenol isomers in aqueous solution. After addition of freshly prepared solution of $NaBH_4$ absorbance peaks of nitrophenol isomers were shifted immediately from 317 to 400, from 350 to 410 and from 330 to 380 for *p*-NP, *o*-NP and *m*-NP, respectively. In $NaBH_4$ medium (pH > 12.0) the peaks corresponding to NP isomers were red shifted due to the formation of nitrophenolate ions.[32] In the absence of any catalyst, the reduction of nitrophenol isomers can be achieved in the presence of $NaBH_4$ but requires more than 7 h, and even in some cases the peak of

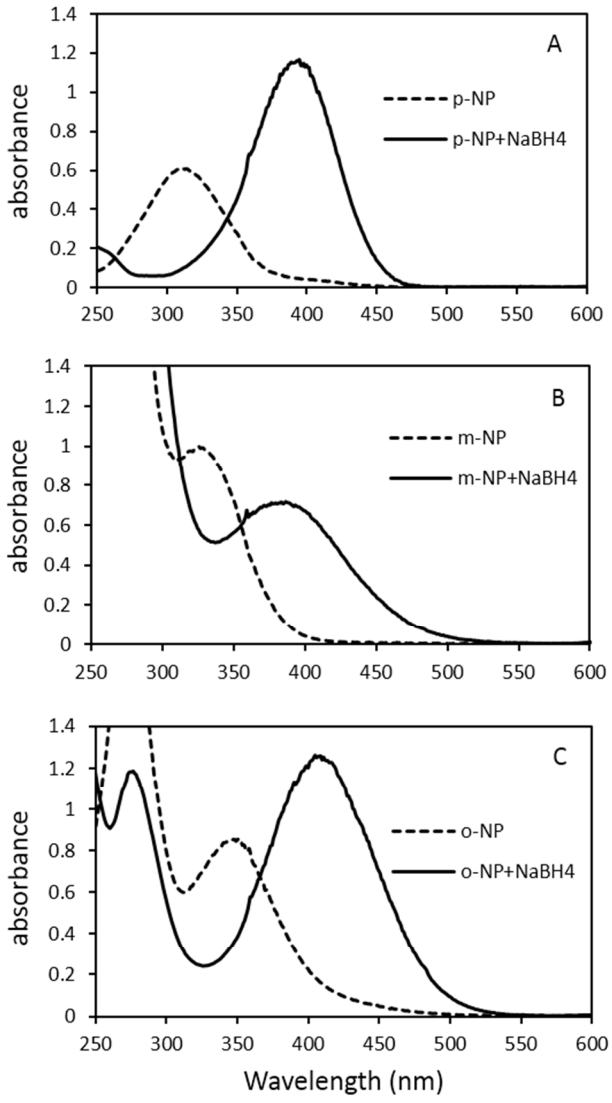

Fig. 2 Absorption spectra for the nitrophenol isomers, and nitrophenol isomers in the presence of 40 mM $NaBH_4$: (A) 8.7mgL^{-1} of *p*-nitrophenol, (B) 67.5 mgL^{-1} of *m*-nitrophenol and (C) 48.2 mgL^{-1} of *o*-nitrophenol.

nitrophenolate ions remained unaltered for a couple of days[33]. However after addition of catalytic amount of gold nanoparticle yellow color of the solution started fading with time and ultimate the color was completely discharged within a few minutes. This is due to the reduction of nitrophenol to aminophenol. When gold nanoparticles is added, the electron donor (BH_4^-) and electron acceptor (nitrophenolate ion) are

adsorbed on the surface of the gold nanoparticles. Subsequently, the catalytic reduction starts by the transfer of electron from BH_4^- to nitrophenolate ions. Thus, gold nanoparticles facilitate the reduction of nitrophenol to aminophenol by lowering the activation energy of the reaction and play the role of catalyst[34].

As shown in Fig. 3A-C, the UV–Vis spectra of discoloration for three isomers were monitored with the progress of the catalytic reductions. Each data set includes successive decrease of the peak height, attributed to the reduced product, aminophenol. Because of monitoring this kinetic process, for each sample a matrix of data was achieved; i.e. creation of second order data. A little $NaBH_4$ is always decomposed in the reaction medium, causing liberation hydrogen, which prevented the aerial oxidation of the products. Since in the present study, the concentration of $NaBH_4$ in the reaction mixture far exceeded the concentration of nitrophenols, it could be considered to remain constant during this reaction and the reactions followed pseudo-first order reaction kinetics.[32] As seen in Fig. 3A-C, the UV–Vis spectra corresponding to the reduction process of nitrophenol isomers have different feature to each other. The normalized absorbance versus time plot, shown in Fig. 3D, more clearly indicates the interesting differences in the kinetics profiles of nitrophenol isomers. The difference in shape and intensity of the time-dependent spectra of the NP reduction processes as well as the kinetics of the process, inspired us to develop a method to determination nitrophenol isomers in the presence of each other.

Quantitation of nitrophenols in mixtures

According to the mentioned difference in kinetic process of three nitophenols, determination procedure can be performed in binary mixtures. Fig. 4A-C shows the typical time-dependent UV–Vis spectra corresponding to the binary mixtures of nitrophenols. The UV–Vis spectra obtained in the kinetic process arranged in a data matrix, denoted as **D**. Rows of the data matrix, **D**, are the UV–Vis spectra recorded at different times and columns of the matrix **D** are the kinetic evolution recorded at different wavelengths. So, such data matrix has a number of rows equal to the number of times and a number of columns equal to the number of wavelengths. In the analysis of these second-order data of nitrophenols mixtures, the following strategy was applied: one of the components is the analyte to be quantified, while the other is considered as an unknown interference. The matrix of the binary mixture is augmented with the matrix of one of the analytes (standard matrix) and simultaneously analyzed. In this procedure, no information

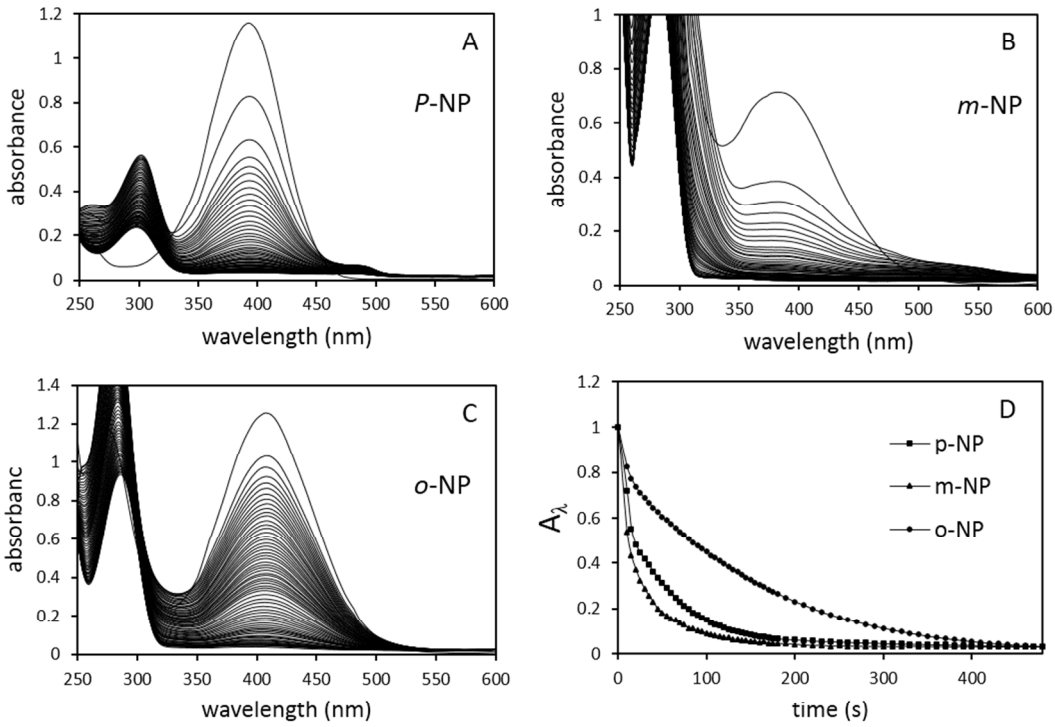

Fig. 3 UV–Vis spectra for successive reduction of nitrophenol isomers catalyzed by gold nanoparticle within 420 s. (A) 8.7mgL^{-1} of p-nitrophenol, (B) 67.5 mgL^{-1} of m-nitrophenol and (C) 48.2 mgL^{-1} of o-nitrophenol. (D) The normalized absorbance versus time plot at wavelength of maximum absorbance for A, B and C kinetic processes. Conditions: [Au_{13}] = 0.04 nM; [$NaBH_4$] = 40 mM; T=25°C; After addition of Au_{13} the first spectrum was recorded at 10 s and after that the spectra were recorded every 5 s to 3 min, and then every 10 s to 8 min.

Journal Name

RSCPublishing

ARTICLE

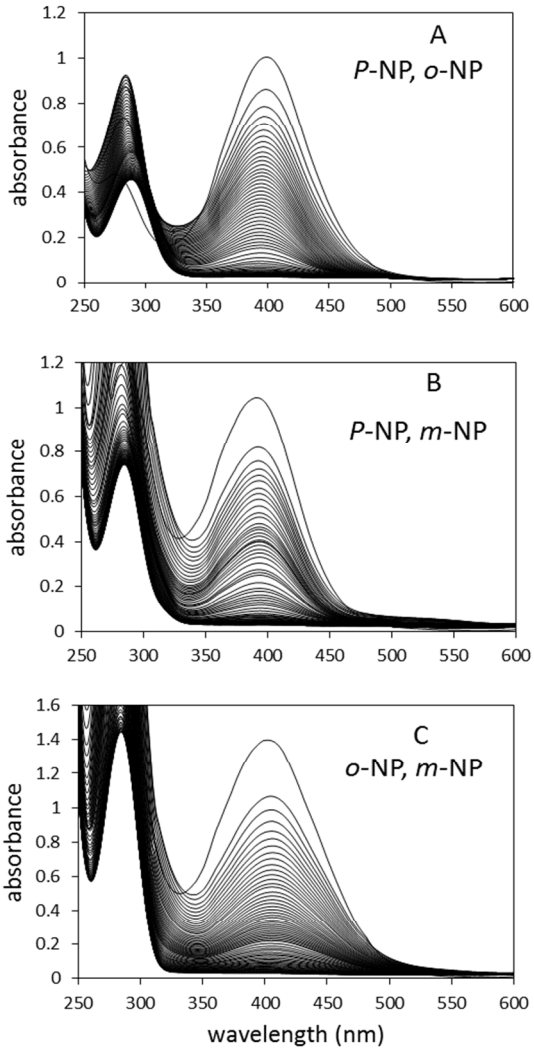

Fig. 4 UV–Vis spectra for successive reduction of nitrophenol mixtures catalyzed by gold nanoparticle within 420 s. (A) 3.8 mgL^{-1} of p-nitrophenol and 19.3 mgL^{-1} of *o*-nitrophenol, (B) 4.3 mgL^{-1} of p-nitrophenol and 38.6mgL^{-1} of *m*-nitrophenol and (C) 38.6mgL^{-1} of *o*-nitrophenol and 38.6mgL^{-1} of m-nitrophenol. Conditions: $[Au_{13}]$ = 0.04 nM; $[NaBH_4]$ = 40 mM; T=25°C; After addition of Au_{13} the first spectrum was recorded at 10 s and after that the spectra were recorded every 5 s to 3 min, and then every 10 s to 8 min.

relative to the interference is introduced, depending on which is the analyte to be quantified.

The analysis was carried out by multivariate curve resolution optimized by alternating least squares (MCR-ALS) as a soft-modeling method. As shown in Fig. 5A, a data matrix includes two components, **D**, is decomposed according to a bilinear model employing MCR-ALS, where **C** is the matrix of the kinetic concentration profiles of the compounds resolved in the analysis of data sample, and S is the matrix of corresponding pure absorbance spectra. The resolved absorbance spectra allow the identification and qualitative information of the coexist compounds. Finally, **E** is the background and noise contribution not modeled by the resolved compounds in **C** and **S**. Decomposition of data matrix to **C** and **S** matrices is performed using multivariate curve resolution methods. Rotational ambiguity problem is inherent to curve resolution methods which needs to pay careful attention.[35] Rotational ambiguity causes to create an infinite number of solutions (**C**, **S**) all of them reconstruct data matrix **D**. Some constraints such as non-negativity of concentration, pure spectra, local rank and selectivity can significantly reduce the range of possible solutions. To deal with rotational ambiguity problem, number of procedures has been proposed to estimate sets of feasible solutions in the case of two and three component mixtures as well as more complex multi-component mixtures.[30, 36, 37] Among different procedures, Vousough et al. introduced a method for obtained all feasible solutions of a data matrix called grid search approach.[38] Using this approach, a range of spectra and concentration profiles of coexistent components is achieved, instead of one of the possible profiles, out coming form MCR-ALS.

The same type of data analysis, based on a bilinear model, can also be carried out simultaneously over several kinetic data (several samples analyzed). As mentioned before, in order to quantitative analysis, the matrix of the binary mixture is augmented with the matrix of standard, and $\mathbf{D}_{aug}$ is created. When the data matrix of the unknown sample is augmented with that of a standard and analyzed simultaneously, quantitative determination of a certain compound in the unknown mixture can be performed, from comparison of the resolved profiles obtained for this compound in each matrix. Once augmented data set is resolved, the information associated to the analyte of interest can be separated from the information companied with the interferent. Since one concentration is known (that is in the standard), the absolute concentration in the unknown sample can be derived easily by comparing the area or height of the resolved profiles of standard and unknown sample:

$$C_{un} = (A_u/A_{std})\, C_{std}$$

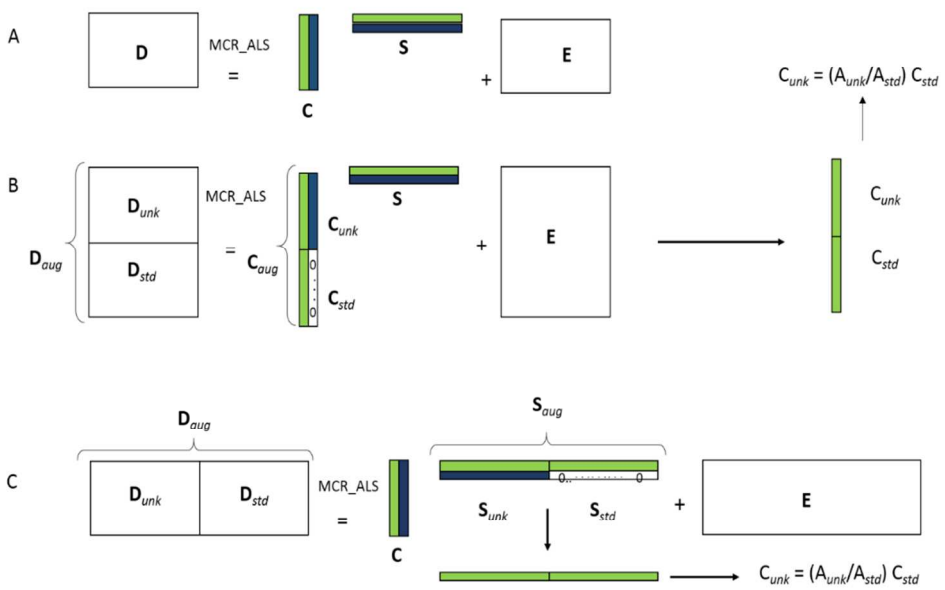

Fig. 5 (A) soft-modelling curve resolution applied to the single data matrix **D**. Possible data matrix arrangements for soft-modelling analysis: (B) column-wise augmented data matrix, (C) row-wise augmented data matrix.

where C_{un} and C_{std} are the concentrations of the analyte in the unknown and standard samples, A_u and A_{std} can be replaced by h_u and h_{std} when using peak height in calculations.

Either resolved concentration profile, $\mathbf{C}_{aug}$, or absorbance profile, $\mathbf{S}_{aug}$, could be used to evaluate the quantitative information, dependent on the type of augmentation of standard and unknown data matrices. There is two types of augmented data; a) column-wise augmented data matrix, setting the corresponding data matrices, one on top of the each other (column data matrix augmentation) and keeping their columns (wavelength) the same for all of them. As shown in Fig. 5B, the new column-wise augmented data matrix, $\mathbf{D}_{aug}$, can be decomposed similarly using the bilinear model equation. This new augmented data matrix, $\mathbf{D}_{aug}$, has a number of rows equal to the total number of times considered for the analysis in the different kinetic processes, and it has a number of columns equal to the number of considered wavelengths. Therefore, $\mathbf{C}_{aug}$ is the augmented matrix of the resolved kinetic concentration profiles in the different kinetic processes, formed by multiple C submatrics (see Fig. 5B). In this case, from resolved concentration profiles, quantitative information can be obtained. **S**, as in Fig. 5A, is the matrix of pure absorbance spectra of the resolved coexisted compounds. Since, in the case of column-wise augmented data matrix, the strategy of augmentation, forces common species to have the same spectrum in two data matrices, the quantitative information of the systems can be found in the $\mathbf{C}_{aug}$. So, the resolved concentration profile is used to determine of unknown concentration. And b) row-wise augmented data matrix arranging the corresponding data matrices **D**, next to the each other (row data matrix augmentation) and keeping their rows (kinetic concentration profile) the same for all of them (see Fig. 5C). In this way, the augmented data matrix, $\mathbf{D}_{aug}$, has a number of rows equal to the number of times considered for the analysis in the individual corresponding kinetic data matrices **D**, and it has a number of columns equal to the total number of considered wavelengths for the analysis in the different kinetic process. Therefore, $\mathbf{S}_{aug}$ is the augmented matrix of the resolved absorbance profiles in the different kinetic process, formed by multiple **S** submatrics. In row-wise augmented data, quantitative information is obtained from resolved spectral profiles. Simultaneous analysis of augmented matrix including the unknown data matrix and pure standard data of the certain compound in the unknown mixture enable us to estimate the concentration of the desired components. About the row-wise augmentation, common species have the same concentration profile in two data matrices and the quantitative information of this system is included in the **S** matrix. Therefor the $\mathbf{S}_{aug}$ is applied to determination purpose.

Determination of *o*-NP. Sample 1 in the Table1 is a representative mixture of *o*-NP with *p*-NP which also was shown in Fig. 5A. The concentration of *o*-NP as the analyte of interest is 19.3 mgL^{-1}, in the presence of 3.9 mgL^{-1} of *p*-NP. This mixture has a maximum absorbance around 400 nm, which shows major contribution of *p*-NP, because of the greater molar absorptivity of *p*-NP rather than the *o*-NP. In order to quantitative estimation of o-NP, data matrix of this sample was augmented with a standard matrix of *o*-NP in column-wise manner, as indicated in Fig. 2B. The part of data between 340 to 465 nm and in the course of 480 s was used to analyze (**D** (66×126)). MCR-ALS started with an initial estimate of pure concentration profiles, which was performed by SIMPLISMA[39]. The imposed constraints were non-negativity

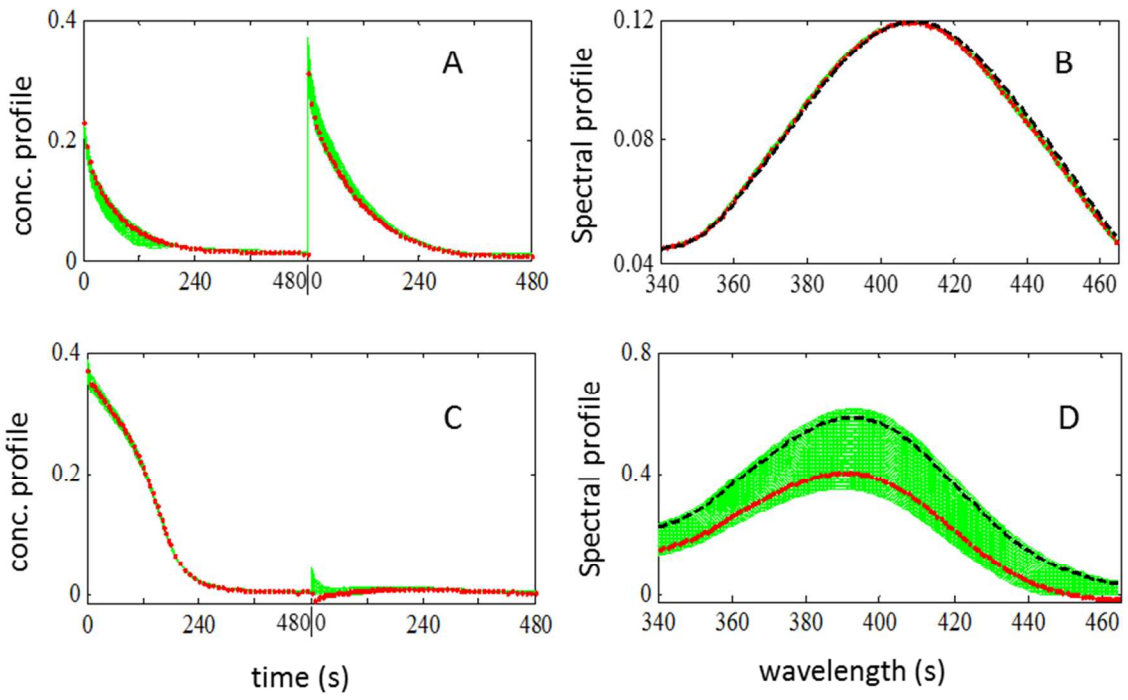

Fig. 6 Plot (A) and (B) are the resolved concentration and spectra profiles of the analyte. (C) and (D) are the resolved concentration and spectra profiles of the interferent; red dots (•) indicate the profiles resolved by MCR-ALS; black dashed line indicates the true spectra profiles and green full line shows the profiles resolved by grid search procedure.

of spectra and concentration profiles, local rank constraint. The local rank constraint in this kind of augmentation was applied to concentration profiles including the zero concentration regions where only there is one (standard) compound in $\mathbf{D}_{std}$ part of $\mathbf{D}_{aug}$. The resolved spectra and concentration profiles for analytes and interferent are demonstrated in Fig. 6A-B and Fig. 6C-D, respectively, which MCR-ALS results are depicted in figures with the red marker '•'. Since the strategy of column-wise augmentation of the data matrices forces common components to have the same spectrum in both data matrices, the quantitative information of the systems is found in the **C** matrix of the augmented data set. Once the kinetic profile of analyte in the mixture was resolved, the concentration related to

Table 1. Quantitative determination of the nitrophenols isomers in binary mixtures.

Sample	Analyte: (mgL^{-1})	Interferent: (mgL^{-1})	MCR-ALS result(%error): (mgL^{-1})	ranges of concentration[a]: (mgL^{-1})
Sample 1	*o*-NP: 19.3	*p*-NP: 3.8	21.2 (9.8)	13.8-23.5
Sample 2	*o*-NP: 38.5	*m*-NP: 38.5	38.8 (0.8)	38.1-39.5
Sample 3	*m*-NP: 38.5	*p*-NP: 4.8	39.3 (2.0)	39.4-63.8
Sample 4	*m*-NP: 48.2	*o*-NP: 48.2	46.5(-3.5)	9.1-65.8
Sample 5	*p*-NP: 7.7	*o*-NP: 7.7	7.8 (1.3)	4.7-7.9
Sample 6	*p*-NP: 1.9	*o*-NP: 1.9	2.0 (5.3)	1.9-2.3
Sample 7	*p*-NP: 3.8	*m*-NP: 5.8	3.6 (-5.3)	2.1- 4.3

[a]Result obtained using grid search procedure

this profile was estimated according to the calibration procedure. In quantitative calculations (based on peak area), concentration value estimated for analyte was 21.2 mgL^{-1}, as seen in Table 1. As mentioned before, the resolved profiles with MCR-ALS are one of the feasible solutions, which related to especial applied initial estimate. So, the calculated value for an analyte concentration is a quantity in search procedure, the ranges of the all feasible solutions for the **C** matrix or kinetic profiles were obtained. The constraints imposed in the examples were the same as the ones applied in the MCR-ALS method. The kinetic and spectra profiles calculated from the feasible regions for analyte and interferent are shown in Fig. 6A-D, as the blue and green curves, respectively. According to the obtained peak area calculations, the possible concentrations of the *o*-NP were obtained between 13.9 mgL^{-1} and 23.5 mgL^{-1}, as presented in last column of Table 1. Sample 2 (in Table 1) is another example of binary mixture of *o*-NP in the presence of *m*-NP. The plot of this data can be seen in Fig. 5C. Similar analytical procedure was applied to this data matrix to determine the concentration of *o*-NP in the presence of *m*-NP. The concentration of *o*-NP in this mixture was 38.5 mgL^{-1} and the predicted concentration of 38.8 mgL^{-1} was obtained using MCR-ALS method. According to determine *o*-NP in several other synthetic mixtures, a prediction ability was found for determination of *o*-NP, in the concentration range from 6.0 to 38.8 mgL^{-1}.

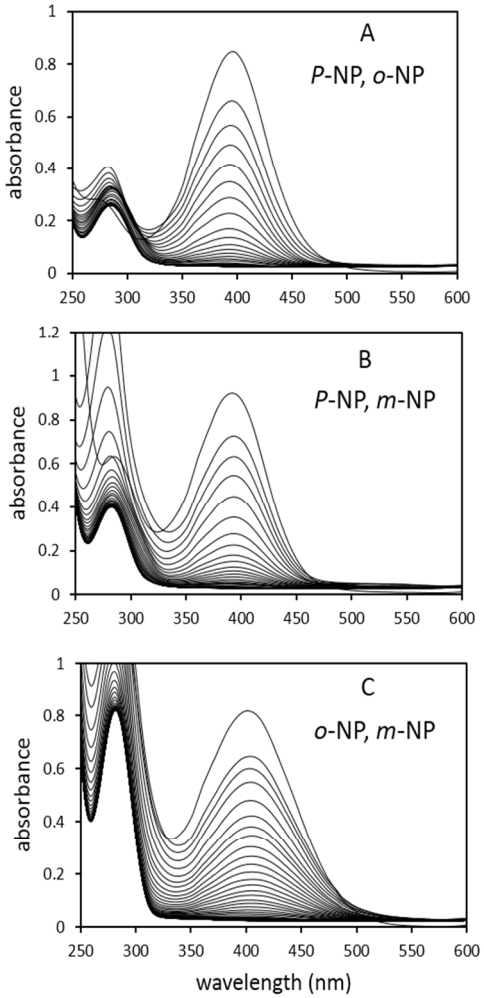

Fig. 7 UV–Vis spectra for successive reduction of binary mixture of nitrophenol isomers in real matrix, catalyzed by gold nanoparticle within 480 s. (A) 4.8 mgL^{-1} of *p*-nitrophenol and 7.7 mgL^{-1} of *o*-nitrophenol (B) 5.8 mgL^{-1} of *p*-nitrophenol and 19.3 mgL^{-1} of *m*-nitrophenol and (B) 19.3 mgL^{-1} of *o*-nitrophenol and 28.9 mgL^{-1} of *m*-nitrophenol. Time intervals are the same for three catalytic reaction. Conditions: $[Au_{13}]$ = 0.04 nM; $[NaBH_4]$ = 40 mM; T=25°C; [NaCl] = 0.1 M; After addition of Au_{13} the first spectrum was recorded at 10 s and after that the spectra were recorded every 5 s to 3 min, and then every 10 s to 7 min.

Determination of *p*- and *m*-NP. Data augmentation in the cases of *p*- and *m*-NP is different than *o*-NP, since more accurate results were achieved in row-wise augmentation. So, quantitative information of the systems was found in the S matrix of the augmented data set (Fig. 5C). The results of MCR-ALS quantitative analysis for *p*- and *m*-NP are summarized in Table 1. Also all the possible concentrations of analytes, which were achieved by grid search procedure, are presented in the last column of Table 1. Herein, an initial estimate of pure spectral profiles, was used to start MCR-ALS. The constraints imposed were non-negativity of spectra and concentration profiles and local rank constraint, which were the same as the ones applied in previous section. The local rank constraint in this kind of augmentation, was applied to spectra profiles including the zero spectra regions, due to the lack of the presence of the interference in the standard samples.
Experimentally, in the case of *m*-NP, the part of data between 345 and 455 nm and in time reaction of 480 s was used for analysis (**D** (66×111)). The employed range of wavelength for determination of *p*-NP was 340 to 445 and the reaction time was 320 s (**D** (50×106)). Analysis of several synthetic mixtures showed a prediction ability in the concentration range between 2.0 - 9.5 mgL^{-1}, and 14.0 - 57.8 mgL^{-1} for *p*- and *m*-NP, respectively.

Determination of the nitrophenol isomers in the real matrix samples

The proposed method was applied to determine the nitrophenol isomers in dam water. No signal was observed for them in dam water, which may be attributed to the lack of nitrophenols in water samples or, this points that, the concentration of nitrophenols were lower than the detection limit. Thus, this method was applied to spiked samples of nitrophenols at certain concentrations. To make the more similar matrix of unknown and standard samples, the kinetic processes were performed in the presence of NaCl solution (0.1 M). Due to increase the ionic strength of reaction medium, the rate of reduction was greater than that in distilled water. **D** matrix in these cases had 50 rows or time point (the reaction time was 320 s). Fig. 7A-C shows the evolution UV–Vis spectra corresponding to binary mixture of spiked nitrophenols in the dam water including 0.1 M NaCl. The kinetic reduction of these unknown and standard samples

Table 2. Quantitative determination of the nitrophenol isomers in binary mixtures with real matrix.

Sample	Analyte: (mgL^{-1})	Interferent: (mgL^{-1})	MCR-ALS result (%error): (mgL^{-1})	ranges of concentration[a]: (mgL^{-1})
Sample 1	*o*-NP: 7.7	*p*-NP: 7.7	8.0 (3.9)	4.5-9.5
Sample 2	*o*-NP: 19.3	*m*-NP: 28.9	18.7 (-3.1)	18.4-19.3
Sample 3	*m*-NP: 27.5	*p*-NP: 9.7	25.1 (9.7)	14.1-57.0
Sample 4	*m*-NP: 43.4	*o*-NP: 19.3	46.2 (6.5)	17.1- 55.6
Sample 5	*p*-NP: 4.8	*o*-NP: 7.7	4.3 (-10.4)	2.7- 5.5
Sample 6	*p*-NP: 5.7	*m*-NP: 19.3	5.3 (-7.0)	3.7-6.3

[a]Result obtained using grid search procedure

were finished completely within 420 s. Nitrophenols samples with real matrix underwent the same analysis procedure. The results of analysis are summarized in Table 2 and show good agreement with true quantities of nitrophenol isomers.

Conclusions

In conclusion, we have taken the benefit of the gold nanoparticles catalytic activity to generate second-order data, during kinetic reduction of NP isomers. These data were used to develop a method to determine the nitrophenol isomers in binary mixtures. Analysis of the mixtures by MCR-ALS provided second-order advantage. This advantage is the quantitation of analytes in the presence of unknown interferences; in contrast to need the complete model of interferences in first-order multivariate calibration methods. As another benefit of second-order data analysis, determination of NPs was performed using single standard data matrix containing the analyte of interest, therefore avoiding a large number of calibration samples. Generally, the described method was very simple and rapid, and the results were in good agreement with true concentrations. In addition, the ranges of possible concentrations of NP isomers (which may be obtained by different initial estimates applied in multivariate curve resolution methods) were calculated for each sample, using grid search procedure. The predicted values of NP concentrations for real samples, showed the high prediction ability of the proposed procedure. To the best of our knowledge, this is the first application of gold nanoparticle catalytic activity to determine the NP isomers in binary mixtures with the second-order advantage.

Notes and references

[a] Faculty of Chemistry, Institute for Advanced Studies in Basic Sciences (IASBS), 45195-1159, Zanjan, Iran.

[b] Department of Chemistry, Sharif University of Technology, Tehran 11155-9516, Iran, and
Institute for Nanoscience and Nanotechnology, Sharif University of Technology, Tehran, Iran.

1 N. Gupta, H. P. Singh and R. K. Sharma, *J. Mol. Catal. A: Chem.*, 2011, **335**, 248.
2 Y. Mikami, A. Dhakshinamoorthy, M. Alvaro and H. García, *Catal. Sci. Tech.*, 2013, **3**, 58.
3 H. J. Parab, H. M. Chen, T.-C. Lai, J. H. Huang, P. H. Chen, R.-S. Liu, M. Hsiao, C.-H. Chen, D.-P. Tsai and Y.-K. Hwu, *J. Phys. Chem. C*, 2009, **113**, 7574.
4 Y. B. Zheng, L. Jensen, W. Yan, T. R. Walker, B. K. Juluri, L. Jensen and T. J. Huang, *J. Phys. Chem. C*, 2009, **113**, 7019.
5 G. Hutchings, *J. Catal.*, 1985, **96**, 292.
6 M. Haruta, N. Yamada, T. Kobayashi and S. Iijima, *J. Catal.*, 1989, **115**, 301.
7 M. D. Hughes, Y.-J. Xu, P. Jenkins, P. McMorn, P. Landon, D. I. Enache, A. F. Carley, G. A. Attard, G. J. Hutchings and F. King, *Nature*, 2005, **437**, 1132.
8 A. Henglein, *Chem. Rev.*, 1989, **89**, 1861.
9 A. Leelavathi, T. U. B. Rao and T. Pradeep, *Nanoscale Res. Lett.*, 2011, **6**, 1.
10 L. Hanne, L. Kirk, S. Appel, A. Narayan and K. Bains, *Appl. Environ. Microbiol.*, 1993, **59**, 3505.
11 U. E. P. Agency, *Fed. Regist*, 1989, **52**, 131.
12 A. Fiorentino, A. Gentili, M. Isidori, P. Monaco, A. Nardelli, A. Parrella and F. Temussi, *J. Agric. Food Chem.*, 2003, **51**, 1005.
13 K.-R. Kim and H. Kim, *J. Chromatogr. A*, 2000, **866**, 87.
14 Y. Tang, R. Huang, C. Liu, L. S. Yang, Z. Z. Lu and S. Luo, *Anal. Methods*, 2013, **5**, 5508.
15 D. A. Perry, H. J. Son, J. S. Cordova, L. G. Smith and A. S. Biris, *J. Colloid Interface Sci.*, 2010, **342**, 311.
16 K. Asadpour-Zeynali and P. Soheili-Azad, *Environ. Monit. Assess.*, 2012, **184**, 1089.
17 Z. Liu, X. Ma, H. Zhang, W. Lu, H. Ma and S. Hou, *Electroanal.*, 2012, **24**, 1178.
18 X. Xu, Z. Liu, X. Zhang, S. Duan, S. Xu and C. Zhou, *Electrochim. Acta*, 2011, **58**, 142.

19 D. A. Fletcher, R. F. McMeeking and D. Parkin, *J. Chem. Inf. Comput. Sci.*, 1996, **36**, 746.
20 Y. N. Ni, C. F. Huanga and S. Kokot, *Chemom. Intell. Lab. Syst.*, 2004, **71**, 177.
21 Y. N. Ni, C. F. Huanga and S. Kokot, *Anal. Chim. Acta,* 2007, **599** 209.
22 R. Tauler, A. K. Smilde and B. R Kowalski, *J. Chemometr.*, 1995, **9**, 31.
23 R. Bro, *Chemom. Intell. Lab. Syst.*, 1997, **38**, 149.
24 E. Sanchez and B. R. Kowalski, *Anal. Chem.*, 1986, **58**, 496.
25 E. Peré-Trepat, S. Lacorte and R. Tauler, *J. Chromatogr A*, 2005, **1096**, 111.
26 N. E. Llamas, M. Garrido, M. S. D. Nezio and B. S. F. Band, *Anal. Chim. Acta*, 2009, **655**, 38.
27 L. A. F. De Godoy, L. W. Hantao, M. P. Pedroso, R. J. Poppi and F. Augusto, *Anal. Chim. Acta*, 2011, **699**, 120.
28 T. Azzouz and R. Tauler, *Talanta*, 2008, **74**, 1201.
29 M. C. Antunes, J. E. J. Simão, A. C. Duarteb and R. Tauler, *Analyst*, 2002, **127**, 809.
30 W. H. Lawton and E. A. Sylvestre, *Technometrics*, 1971, **13**, 617.
31 G. Frens, *Nature*, 1973, **241**, 20.
32 S. Jana, S. K. Ghosh, S. Nath, S. Pande, S. Praharaj, S. Panigrahi, S. Basu, T. Endo and T. Pal, *Appl. Catal. A*, 2006, **313**, 41.
33 N. Pradhan, A. Pal and T. Pal, *Colloids Surf. A*, 2002, **196**, 247.
34 S. A. Aromal and D. Philip, *Spectrochim. Acta A*, 2012, **97,** 1.
35 G. Ahmadi and H. Abdollahi, *Chemom. Intell. Lab. Syst.*, 2013, **120,** 59.
36 O. S. Borgen, N. Davidsen, Z. Mingyang and Ø. Øyen, *Microchim. Acta*, 1986, **89**, 63.
37 R. Rajkó and K. István, *J. Chemometr.*, 2005, **19**, 448.
38 M. Vosough, C. Mason, R. Tauler, M. Jalali-Heravi and M. Maeder, *J. Chemometr.*, 2006, **20**, 302.
39 W. Windig and J. Guilment, *Anal. chem.*, 1991, **63**, 1425.

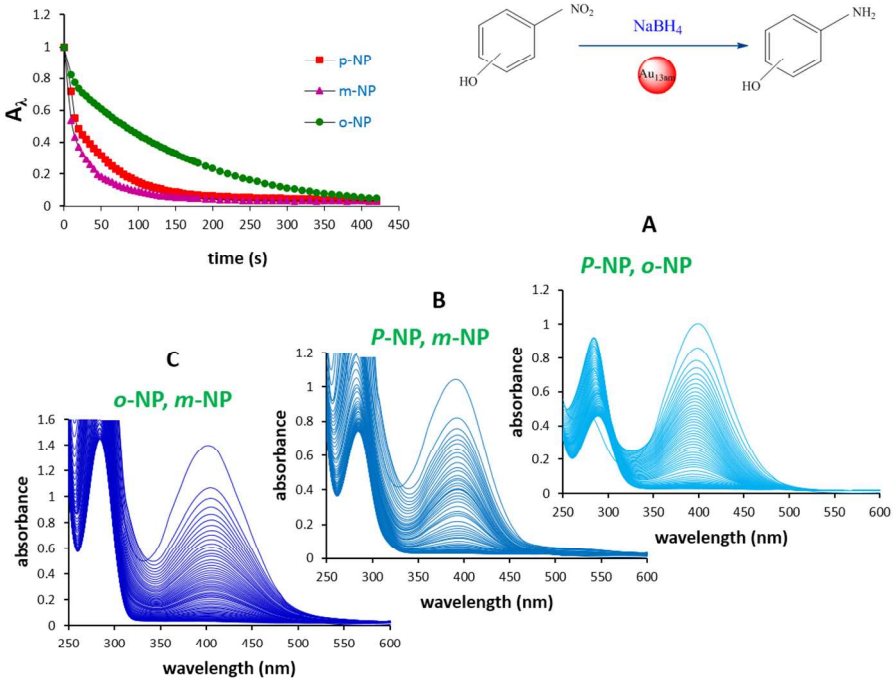

223x173mm (150 x 150 DPI)